Monitoring twenty-first century climate using GPS radio occultation bending angles

Mark A. Ringer[1] and Sean B. Healy[2]

1 Met Office, Exeter, U.K.
2 ECMWF, Reading U.K.

18 October 2007

Corresponding author:

Dr Mark A. Ringer
Met Office
Hadley Centre for Climate Change
FitzRoy Road
Exeter EX1 3PB
United Kingdom

Tel: +44 (0)1392 884202
Fax: +44 (0)1392 885681
E-mail: mark.ringer@metoffice.gov.uk

(Submitted to Geophysical Research Letters)

Abstract

Simulations of radio occultation bending angle profiles in transient climate experiments using a state-of-the-art global coupled climate model show a clear signal in bending angle emerging over the first half of the twenty-first century. The bending angle signal can be related to the predicted changes in the climate over this period in response to increasing greenhouse gas concentrations and is shown to be primarily a combination of three distinct effects: the changing temperature structure of the atmosphere, increased water vapor in the troposphere, and the expansion of the atmosphere due to the warming. Analysis of the predicted trends in the bending angle indicates that the climate change signal in the tropical upper troposphere and lower and middle stratosphere may become distinguishable from natural variability, i.e. “detected”, after approximately ten to sixteen years of measurements. This suggests that such observations may be one of our best prospects for monitoring the evolution of the climate over the coming decades.

1. Introduction

Accurate, global, and stable long-term observations are the key to understanding the changes in climate over the coming decades predicted by the current generation of global climate models (GCMs). These observations will provide direct evidence of the climate's evolution and will also be essential to evaluate and refine the GCM predictions. GPS radio occultation (RO) measurements possess the necessary characteristics of such an observational record. In addition, their all-weather capability (the measurement is unaffected by clouds, for example), self-calibration (through their traceability to absolute standards) and high vertical resolution mean that they should be capable of providing a climate record that is free from many of the problems associated with both satellite and conventional measurements [*Goody et al.*, 1998].

The RO technique [e.g. *Kursinski et al.*, 1997] is based on the fact that the path of a radio signal propagating between a GPS satellite and a receiver placed on a low earth orbit (LEO) satellite is bent or refracted by the atmosphere. The bending is caused by gradients in the refractive index of the atmosphere, which in turn can be related to gradients in the atmospheric density and water vapour. During an occultation event the motion of the satellites enables the variation of ray bending as a function of minimum ray-height above the surface to be determined. Fundamentally, the RO technique is based on the precise measurement of time-delays with atomic clocks. The bending angles are derived from these delays. Bending angle profiles can then be inverted to provide vertical profiles of refractivity, and subsequently pressure and temperature.

The potential of RO measurements for both climate monitoring and climate model evaluation was described by *Yuan et al.* [1993] and *Kursinski et al.* [1997], who noted in particular that RO observations should be able to provide useful information relating to near-tropopause temperature changes, humidity changes in the lower and middle troposphere, and the expansion of the troposphere due to global warming.

Eyre [1994] outlined how RO data could be exploited by a global numerical weather prediction (NWP) system and concluded that direct assimilation of the bending angle was preferable to using either refractivity profiles or retrievals of temperature and humidity. The benefits of assimilating bending angle measurements in an operational framework have recently been demonstrated by *Healy and Thépaut* [2006], who showed clear improvements in upper tropospheric and lower stratospheric temperatures in experiments using the ECMWF global forecasting system. An important feature of the RO measurement is that it can be assimilated without the need for bias correction. This enhances their ability to correct model biases which are otherwise difficult to rectify because other satellite data tend to be bias corrected to the assimilating model [*Healy and Thépaut*, 2006].

Much work on the climate applications of RO data has focussed on the use of retrieved parameters such as temperature or geopotential heights for climate monitoring [e.g. *Gobiet et al.*, 2007; *Leroy*, 1997]. Recently *Leroy et al.* [2006] have considered the use of “dry pressure”, which can be derived from refractivity profiles, as a potential climate monitoring parameter. However, these derived quantities are more sensitive to structural uncertainty than bending angles [*von Engeln*, 2006] because of the introduction of a-priori information in the additional processing steps [*Eyre*, 1987]. The more fundamental nature of the bending angle measurement, together with its demonstrated utility in the NWP context, suggests the use of the bending angle profile itself as a climate variable. This study therefore considers the use of the bending angle for climate monitoring. By simulating bending angle profiles in a state-of-the-art climate model we explore the climate signal over the next half-century and the information content of this signal in relation to changes in the atmosphere due to climate warming. We also estimate the time required to detect trends in the bending angle over the coming decades.

2. Climate model description and methodology

The climate model used for the bending angle simulations is the Hadley Centre Global Environmental Model, version 1 (HadGEM1), described in *Johns et al.* [2006] and *Martin et al.* [2006]. The atmospheric component of HadGEM1 uses a horizontal resolution of 1.25º latitude × 1.875º longitude and has 38 vertical levels, extending to a height of over 39 km. The zonal resolution of the oceanic model is 1º, while the meridional resolution is 1º between the poles and 30ºN/S, increasing smoothly to 1/3º at the equator. There

are 40 unevenly spaced vertical levels in the ocean, with the resolution near the surface being 10 m. HadGEM1 includes improved physical parameterizations, increased functionality and higher resolution (horizontal and vertical, in the atmosphere and ocean) compared to its predecessor, HadCM3. The atmospheric component uses a new semi-Lagrangian dynamical core and in addition to an almost completely new suite of physical parameterizations includes additional processes such as the sulphur cycle and cloud aerosol effects.

To investigate the climate change signal over the twenty-first century we use a transient coupled model integration following the SRES A1B scenario [*Nakicenovic and Swart*, 2000], which specifies time-varying greenhouse gas and ozone concentrations, aerosol emissions and land use changes over the period 2000-2100. Under this scenario the global mean temperature increase by 2050, relative to the 1961-1990 mean, is approximately 2 K, rising to around 3.6 K by 2100 [*Stott et al.*, 2006]. For reference, the equilibrium climate sensitivity and transient climate response of HadGEM1 (due to doubling of CO_2) are 4.4 K and 1.8 K respectively. We also make use of a long control integration of HadGEM1 (employing fixed greenhouse gases, etc) which has currently completed almost 1300 years and a simulation over the twentieth century which, in addition to greenhouse gases, ozone, aerosols and land use changes, also includes time varying forcings due to volcanic aerosols and solar irradiance changes. The full details of these simulations are given in *Stott et al.* [2006].

The bending angle profiles are calculated from monthly mean fields of temperature, pressure and humidity over the period of interest. So, for the A1B scenario integration, bending angle profiles are calculated at each grid point, for every month over the period from 2000-2055. Given the observed impact parameter, a, the bending angle, α, can be written as [e.g. *Kursinski et al.*, 1997]

$$\alpha(a) = -2a\int_a^\infty \frac{d(\ln n)/dx}{\sqrt{x^2 - a^2}}dx,$$

where n is the refractive index and $x = nr$, with r the radius value of a point on the ray path. The refractive index is derived from the climate model fields using

$$N = 10^6(n-1) = \frac{c_1 P}{T} + \frac{c_2 P_w}{T^2},$$

where N is the refractivity, P is the atmospheric pressure (hPa), T is the temperature (K) and P_w (hPa) is the water vapor partial pressure. The empirical constants c_1 and c_2 are 77.6 K hPa^{-1} and 3.73 × 10^5 K^2 hPa^{-1} respectively. The bending angles are calculated at a fixed set of 110 "impact heights" (defined as the impact parameter minus the local radius of curvature), equally spaced at 250 m intervals in the vertical. This is comparable to the number of impact heights used for assimilation of the data and should be sufficient to demonstrate the information content of the bending profiles in the climate context. Full details of the forward model and the calculation of bending angle profiles from model fields are given in *Healy and Thépaut* [2006].

For reference the annual, zonal mean bending angle profile distribution is shown in Fig. 1(a). The values correspond to around 1 degree at the surface, falling to around 10^{-2} degrees in the middle stratosphere. The sign convention is chosen so that positive values of α indicate bending towards the Earth's surface. As mentioned above, the bending angle profile depends on the atmospheric density: thus from the mid-troposphere upwards the primary dependence is on temperature and pressure, while in the lower troposphere water vapour also makes a significant contribution.

3. Results

Figures 1(b)-(f) show the evolution of the climate change signal from the present-day through to the 2050s as seen in the zonal mean bending angle profiles. The signal in the tropical lower stratosphere emerges after a decade, is clearly identifiable by the 2020s and continues to intensify through to the 2050s. It is accompanied

by a signal in the tropical mid-stratosphere which, though weaker initially, is of comparable size by the 2050s. The signals at polar latitudes in the mid-stratosphere appear to be more variable over the first twenty to thirty years and are not clearly established until the 2040s. In the upper troposphere a signal of opposite sign emerges, the upper boundary of which follows the zonal variation of the height of the tropopause: this delineates the warming of the troposphere due to increased greenhouse gases from the cooling of the stratosphere. In the lower troposphere the increased water vapor as the climate warms appears to dominate and the bending angle signal is positive.

Thus by the 2050s a clear signal in the bending angle, with a well-defined geographical distribution, has emerged. We now wish to investigate the contributions to this signal from the different effects associated with the changing climate over this period. To do this we use the tangent linear version [e.g. *Hoffman et al.*, 1992] of the bending angle forward model. The tangent linear allows us to identify the contributions to the bending angle signal from changes in temperature, pressure and humidity: it calculates the change in the simulated bending angle values produced by pressure, temperature and humidity perturbations for a given linearization state.

The decomposition of the 2050s minus 2000s bending angle differences is calculated with the tangent linear, using the 2000s as the linearization state (Fig. 2). As might have been expected, the contribution to the bending angle signal from the humidity change (Fig. 2a) is confined to the middle and lower troposphere and is largest in tropics, where the atmospheric water vapour abundance is greatest. The temperature change contribution (Fig. 2b) reflects the well-known effect of tropospheric warming and stratospheric cooling due to increasing greenhouse gas concentrations. The basic features of the temperature trends in the present simulations are consistent with the earlier Hadley Centre model study of *Butchart et al.* [2000]. The warming is larger in the upper troposphere than in the lower troposphere, particularly in the tropics – a consequence of the moist adiabatic lapse rate decreasing with the increasing temperatures. Also apparent is the amplification of the surface and tropospheric warming at high latitudes in the Northern Hemisphere. In the stratosphere it is the cooling which increases with altitude: in the lower stratosphere the cooling due to increased longwave emission is to a large degree offset by increased absorption of upwelling longwave radiation from the troposphere. Another feature of note is the warming signal at polar latitudes in both hemispheres at around 18 km. In the Southern Hemisphere this is partly due to the recovery of stratospheric ozone under the prescribed A1B scenario. A possible explanation for the remainder of this signal (and that in the Northern Hemisphere) is dynamical heating due to increased troposphere-stratosphere mass exchange driven by more vigorous extra-tropical tropospheric wave activity [*Butchart and Scaife*, 2001]. The contribution from pressure changes (Fig. 2c) arises from the expansion of the atmosphere as the climate warms [*Kursinski et al.*, 1997; *Leroy et al.*, 2006]: this manifests itself as an increase in pressure at fixed height surfaces, with the maximum (which is around 3-4 hPa in these simulations) occurring near the tropopause.

It can therefore be seen that the total bending angle signal due to climate change can be neatly decomposed into components due to these different effects and results from their linear combination (cf. Figs. 2d and 1f, which indicates that we are within the linear regime with respect to perturbations considered here). In the tropics, for example, we see four distinct maxima: a positive signal due to increasing water vapour in the lower troposphere (which dominates a negative change due to the increased temperature); a negative signal in the upper troposphere due to enhanced warming compared to the surface; a positive signal in the lower stratosphere (due predominantly to the maximum in the thermal expansion effect); and a positive signal in the mid-stratosphere arising primarily from the enhanced radiative cooling compared to the lower stratosphere. Thus, although it might initially appear to be a somewhat esoteric quantity, changes in the bending angle due to climate warming can be readily understood and interpreted in terms of more familiar geophysical variables. Given the particular qualities of the measurement this suggests that the bending angle itself is of great potential use both for climate monitoring and climate model evaluation.

We next consider the application of bending angle measurements to detect climate trends over the coming decades. Following *Weatherhead et al.* [1998], the number of years, n^*, required to detect a trend of magnitude $|\omega_0|$ at the 95% confidence level, with 90% probability is given by

$$n^* = \left[\frac{3.3\sigma_N}{|\omega_0|} \sqrt{\frac{1+\phi}{1-\phi}} \right]^{2/3},$$

where σ_N is the month-to-month variability in the noise and ϕ is the lag 1-month autocorrelation in the noise. This method has previously been applied to total column ozone data [*Weatherhead et al.*, 2000] and to shortwave radiative flux measurements [*Loeb et al.*, 2007].

We consider the trends at the equator at impact heights of 12, 20 and 26 km, where maxima in the bending angle signal have been noted (Fig. 1f). The least squares linear trends are calculated from the A1B scenario integration over the period 2000-2050 (Figs. 3a-c). The variability and autocorrelation in the noise are obtained from the long control integration of HadGEM1 with fixed greenhouse gases and other forcings: monthly mean bending angle profiles are calculated from a set of five fifty-year segments of the simulation and the noise characteristics derived from the monthly mean anomalies after removal of the mean seasonal cycle. The results (Table 1) indicate that the trend in the mid-stratosphere would be detectable within a decade, while those in the lower stratosphere and upper troposphere would be detectable after approximately sixteen years. The 95% confidence intervals in the detection times are given by $(n^* e^{-B}, n^* e^{B})$, where

$$B = \frac{4}{3\sqrt{M}} \sqrt{\frac{1+\phi}{1-\phi}}$$

and M is the number of months of data [*Weatherhead et al.*, 1998]. Alternatively, one can also consider the evolution of the trend estimate with time over the 2000-2050 period (Figs. 3d-f). Here the trend has been estimated using a weighted least squares regression, with the error covariance matrix defined by the estimates of the noise characteristics. In all three cases the trend estimate has clearly started to converge to its final value by the detection times shown in Table 1. Note that these detection times are comparable to estimates presented by *Leroy et al.* [2006] based on the optimal finger-printing technique using dry pressure.

As a caveat to these results it should be noted that if the model's natural variability is unrealistically low (e.g. in the stratosphere due to the relatively low vertical resolution) then these detection limits might be underestimated. On the other hand, it should also be noted that we have not averaged the data in either latitude or height in order to try and reduce the noise. Unpredictable events such as large volcanic eruptions also have the potential to increase the detection times. To test this we have calculated the noise characteristics for the period 1950-2000 using a HadGEM1 simulation employing anthropogenic and observed forcings, including those due to major volcanic events and solar variability. The increase in both the variability and autocorrelation of the noise (primarily due to the eruptions of El Chichón in 1982 and Pinatubo in 1991) leads to potential increases in the detection times of approximately 8-10 years.

4. Conclusions

This study indicates that the emerging signal of climate change due to global warming over the coming decades should be clearly identifiable in radio occultation bending angle profile measurements. Moreover, the bending angle signal can be related, in a straightforward manner, to the predicted changes in the atmospheric structure as the climate warms. Analysis of the predicted trends in bending angle in the tropics suggests that it might be possible to detect climate change signals at key locations in the upper troposphere and in the lower and mid-stratosphere within ten to sixteen years. Given the many difficulties associated with establishing a temperature record of the recent past for the tropical upper troposphere and lower stratosphere [*Karl et al.*, 2006], radio occultation measurements offer an alternative which is highly accurate and free of the calibration issues associated with both conventional observations and other satellite retrievals. Data from the CHAMP mission [*Wickert et al.*, 2001] extend from 2001 to the present and are now being augmented by the more recent COSMIC [*Anthes et al.*, 2000] and GRAS [*Luntama et al.*, 2007] missions. The creation of a bending angle climate record from these data, which will be greatly aided by a thorough knowledge of their error characteristics gained from their use in numerical weather prediction, will provide a powerful new tool for monitoring the evolution of the climate. It will also be an important new resource for testing climate

models and evaluating their predictions of climate change.

Acknowledgments. MAR was supported by the Joint Defra and MoD Programme, (Defra) GA01101 (MoD) CBC/2B/0417_Annex C5. SBH is funded by the GRAS-SAF. We thank Adam Scaife and Gareth Jones for useful discussions during the course of this work. The bending angle forward model used here is available as part of the ROPP software package from the GRAS-SAF homepage (garf.grassaf.org).

References

Anthes R., C. Rocken, and Y.-H. Kou (2000), Applications of COSMIC to meteorology and climate, *Terr., Atmos. Ocean. Sci., 11*, 115 – 156.

Butchart, N. et al. (2000), The response of the stratospheric climate to projected changes in the concentrations of well-mixed greenhouse gases from 1992 to 2051, *J. Climate, 13*, 2142 – 2159.

Butchart, N. and A.A. Scaife (2001), Removal of chlorofluorocarbons by increased mass exchange between the stratosphere and troposphere in a changing climate, *Nature, 410*, 799 – 802.

Eyre, J.R. (1987), On systematic errors in satellite sounding products and their climatological mean values, *Q. J. R. Meteorol. Soc., 113*, 279 – 292.

Eyre, J. (1994), Assimilation of radio occultation measurements into a numerical weather prediction system, Technical Memorandum 199, ECMWF, Reading, U.K.

Gobiet, A. et al. (2007), Retrieval of temperature profiles from CHAMP for climate monitoring: intercomparison with Envisat MIPAS and GOMOS and different atmospheric analyses, *Atmos. Chem. Phys., 7*, 3519 – 3536.

Goody, R., J. Anderson, and G. North (1998), *Testing climate models: an approach, Bull. Am. Meteorol. Soc., 79*, 2541 – 2549.

Healy, S.B. and J.-N. Thépaut (2006), Assimilation experiments with CHAMP GPS radio occultation experiments, *Q. J. R. Meteorol. Soc., 132*, 605 – 623.

Hoffman, R.N., J.-F. Louis, and T. Nehrkorn (1992), A method for implementing adjoint calculations in the discrete case. Technical Memorandum 184, ECMWF, Reading, U.K.

Johns, T.C. et al. (2006), The new Hadley Centre climate model HadGEM1: Evaluation of coupled simulations, *J. Climate, 19*, 1327 – 1353.

Karl, T.R. et al. (Eds) (2006), Temperature trends in the lower atmosphere. Steps for understanding and reconciling differences, Climate Change Science Program, Washington, D.C.

Kursinski, E.R. et al. (1997), Observing Earth's atmosphere with radio occultation measurements using the Global Positioning System, *J. Geophys. Res., 102*, 23429 – 23465.

Leroy, S.S. (1997), Measurement of geopotential height by GPS radio occultation, *J. Geophys. Res., 102*, 6971 – 6986.

Leroy, S.S., J.G. Anderson, and J.A. Dykema (2006), Testing climate models using GPS radio occultation: a sensitivity analysis, *J. Geophys. Res., 111*, D17105, doi:10.1029/2005JD006145.

Loeb, N.G. et al. (2007), Multi-instrument comparison of top-of-atmosphere reflected solar flux, *J. Climate, 20*, 575 – 591.

Luntama, J.-P., et al., (2007), EPS GRAS mission for operational radio occultation measurements. Submitted to Bull. Am. Meteorol. Soc.

Martin, G.M. et al. (2006), The physical properties of the atmosphere in the new Hadley Centre Global Environmental Model, HadGEM1. Part 1: Model description and global climatology, *J. Climate, 19*, 1274 – 1301.

Nakicenovic, N. and R. Swart (Eds.) (2000), Emission Scenarios, Cambridge University Press, 570 pp.

Stott, P.A., et al. (2006), Transient climate simulations with the HadGEM1 climate model: causes of past warming and future climate change, *J. Climate, 19*, 2763 – 2782.

von Engeln, A. (2006), A first test of climate monitoring with radio occultation instruments: comparing two processing centers, *Geophys. Res., Lett.*, 33, L22705, doi:10.1029/2006GL027767.

Weatherhead, E.C. et al. (1998), Factors affecting the detection of trends: statistical considerations and applications to environmental data, *J. Geophys. Res., 103*, 17149 – 17161.

Weatherhead, E.C. et al. (2000), Detecting the recovery of total column ozone, *J. Geophys. Res., 105*, 22201 – 22210.

Wickert, J. et al. (2001), Atmosphere sounding by GPS radio occultation: first results from CHAMP, *Geophys. Res. Lett., 28*, 3263 – 3266.

Yuan, L. et al. (1993), Sensing climate change using the global positioning system, *J. Geophys. Res., 98*, 14925 – 14937.

Table 1: Bending angle trends and detection times at the equator for three selected altitudes.

Impact height (km)	Trend, ω_0 (10^{-6} radians/year)	Variability of noise, σ_N (10^{-6} radians)	Autocorrelation of noise, φ	Detection time, n^* (years)	95% confidence interval (years)
12	-0.92	9.45	0.58	16.3	(14.6, 18.2)
20	1.09	9.20	0.68	16.0	(13.6, 18.7)
26	0.41	2.04	0.55	10.6	(9.4, 11.7)

Figure captions

Figure 1

(a) The annual, zonal mean bending angle profile for 2000 – 2005. (b) – (f) Evolution of the annual mean bending angle climate change signal from the 2010s to 2050s relative to the 2000 – 2005 mean. The signal for the 2010s is the difference between the 2010 – 2015 mean minus the 2000 – 2005 mean, for the 2020s it is the difference between the 2020 – 2025 mean minus the 2000 – 2005, etc.

Figure 2

The contribution to the 2050s bending angle signal from (a) humidity, (b) temperature and (c) pressure and their sum (d).

Figure 3

(a) – (c) Time series of monthly mean bending angle (seasonal cycle removed) at the equator at impact heights of 12, 20 and 26 km over the period 2000 – 2050. The dashed line shows the least squares linear trend. (d) – (f) Evolution of the bending angle trend with time at the same locations. The dashed vertical line indicates the detection times shown in Table 1.

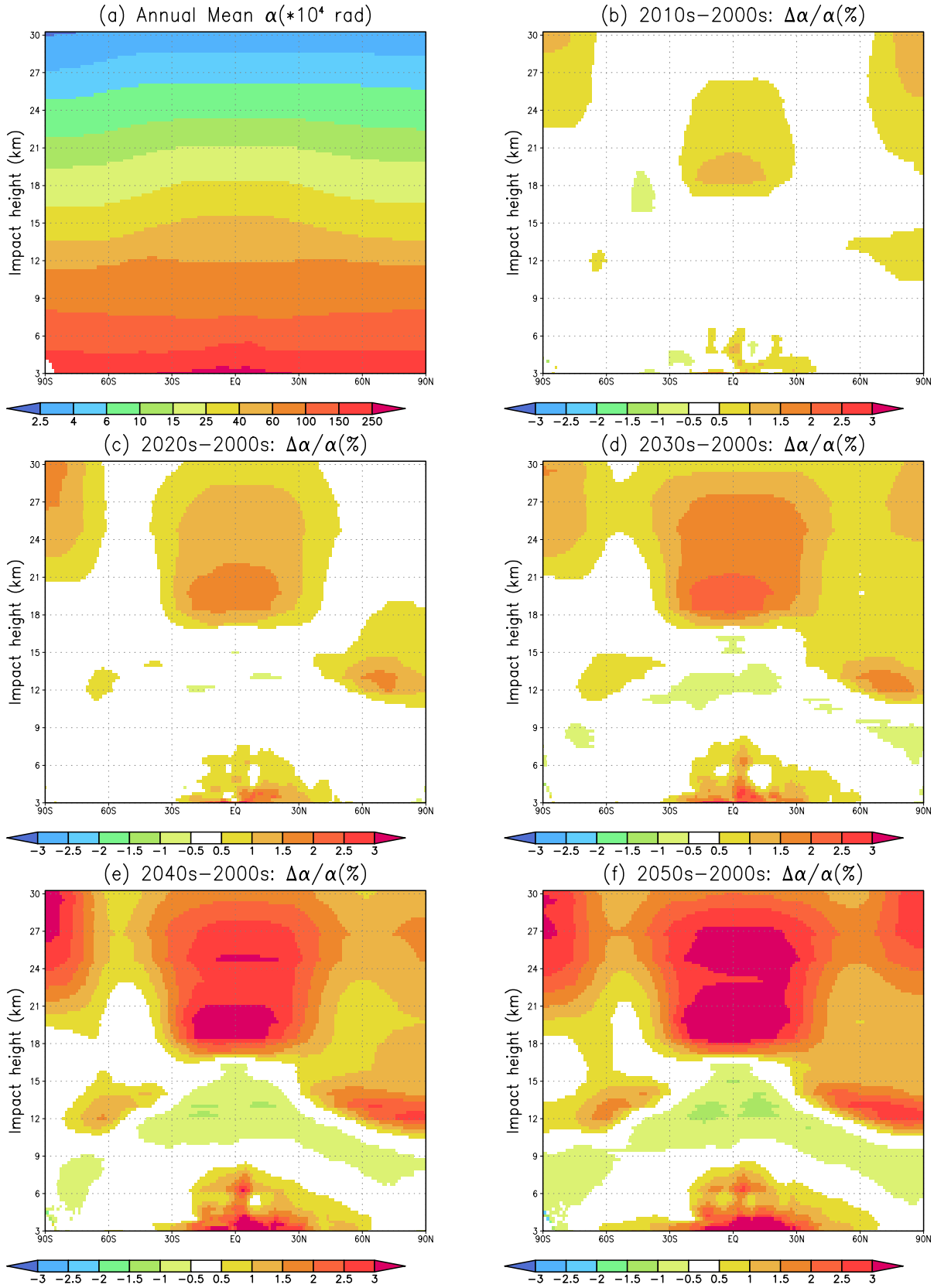
(a) Annual Mean α(*10⁴ rad)
(b) 2010s−2000s: Δα/α(%)
(c) 2020s−2000s: Δα/α(%)
(d) 2030s−2000s: Δα/α(%)
(e) 2040s−2000s: Δα/α(%)
(f) 2050s−2000s: Δα/α(%)
Impact height (km)
90S 60S 30S EQ 30N 60N 90N
2.5 4 6 10 15 25 40 60 100 150 250
−3 −2.5 −2 −1.5 −1 −0.5 0.5 1 1.5 2 2.5 3

Figure 1

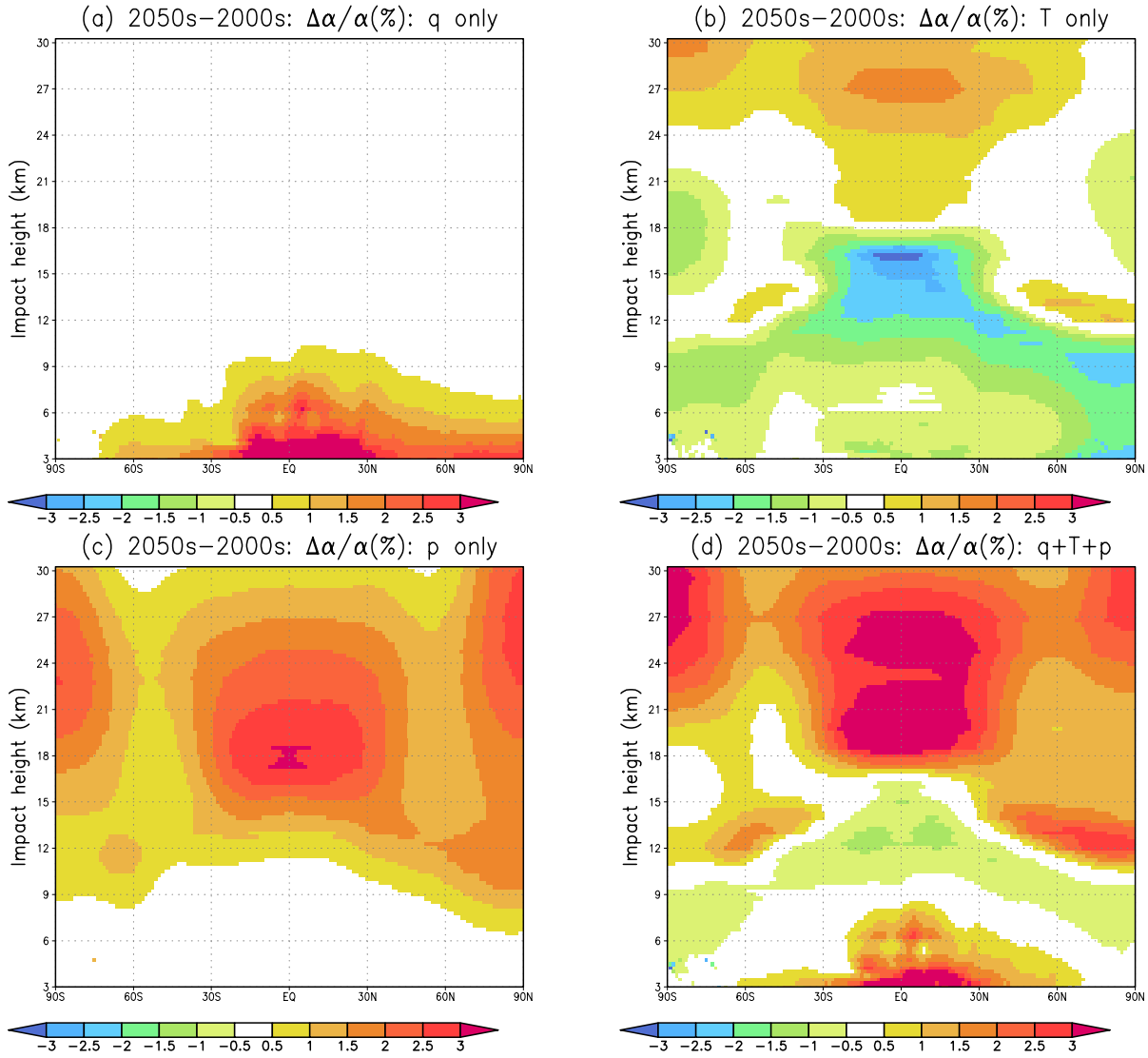
(a) 2050s−2000s: Δα/α(%): q only
(b) 2050s−2000s: Δα/α(%): T only
(c) 2050s−2000s: Δα/α(%): p only
(d) 2050s−2000s: Δα/α(%): q+T+p
Impact height (km)
30
27
24
21
18
15
12
9
6
3
90S
60S
30S
EQ
30N
60N
90N
−3 −2.5 −2 −1.5 −1 −0.5 0.5 1 1.5 2 2.5 3

Figure 2

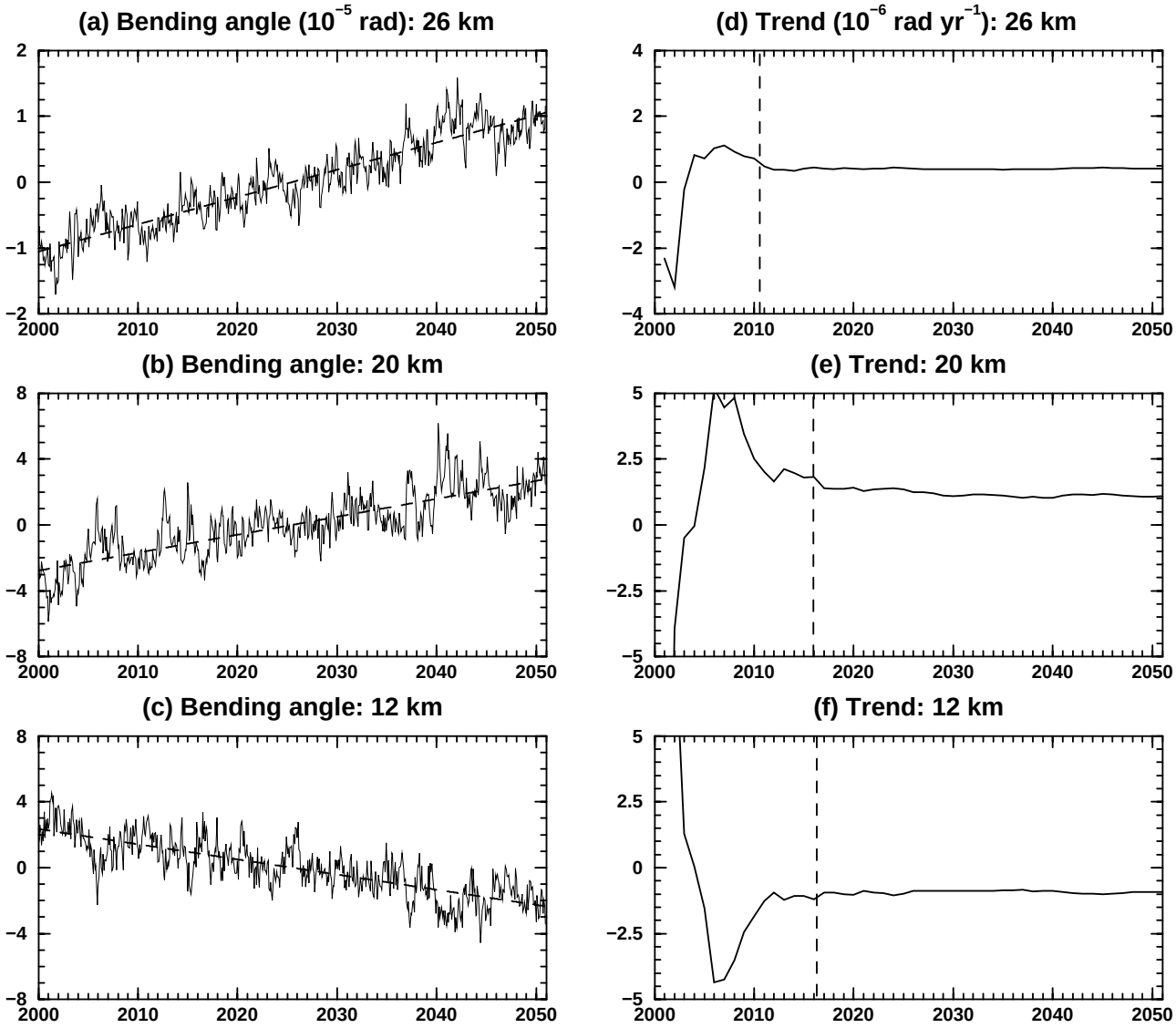
(a) Bending angle (10^−5 rad): 26 km
(d) Trend (10^−6 rad yr^−1): 26 km
(b) Bending angle: 20 km
(e) Trend: 20 km
(c) Bending angle: 12 km
(f) Trend: 12 km
2000
2010
2020
2030
2040
2050

Figure 3